PERGAMON

Acta mater. Vol. 47, No. 8, pp. 2417–2430, 1999

Printed in Great Britain
PII: S1359-6454(99)00095-6
1359-6454/99 $20.00 + 0.00

AN EXPERIMENTAL STUDY OF SPHERICAL INDENTATION ON PIEZOELECTRIC MATERIALS

U. RAMAMURTY†, S. SRIDHAR‡, A. E. GIANNAKOPOULOS§ and S. SURESH

Department of Materials Science and Engineering, Massachusetts Institute of Technology, Cambridge, MA 02139, U.S.A.

(Received 9 December 1998; accepted 16 March 1999)

Abstract—The response of lead zirconate titanate and barium titanate piezoelectric ceramics to spherical microindentation was investigated. Force vs penetration depth curves obtained from instrumented indentation reveal that the indentation stiffness depends on the material condition (i.e. poled vs unpoled) and the type of indentor (i.e. electrically conducting vs insulating). Good agreement was found between the experimental results and predictions of an analytical model of Giannakopoulos and Suresh (1999) for the spherical indentation of a transversely isotropic piezoelectric material. A parametric analysis was conducted to identify key material properties that influence the indentation response. An error analysis was performed so as to assess the influence of the variabilities in constituent properties on the scatter in the measured indentation stiffness. This indentation method has been shown to offer a new methodology for characterizing some properties of piezoelectric materials. Advantages and limitations of such a technique are discussed. © *1999 Acta Metallurgica Inc. Published by Elsevier Science Ltd. All rights reserved.*

Keywords: Indentation; Ceramic, functional; Electrical properties, piezoelectricity; Mechanical properties, elastic; Non-destructive testing

1. INTRODUCTION

Piezoelectric solids exhibit a first order coupling between mechanical stress and electrical potential [1, 2]. Because of this coupling, they are being considered in a growing number of applications in sensors, ultrasonic transducers, actuators, and smart structures [2]. Most of the prior work on piezoelectric materials has focused on developing materials or devices with improved functional or performance characteristics (such as high dielectric and coupling constants) [2, 3]. Some examples include the development of piezoelectric thin films and polymer–matrix composites comprising piezoelectric fibers [2, 4].

The properties of piezoelectric ceramics are sensitive to the presence of impurities and microstructural features such as grain size and porosity [3]. In addition to these factors, they depend on the processing methodology and show systematic and statistical fluctuations within a given batch [3]. The latter arise due to any of the following factors: (i) improper mixing of the raw materials, (ii) variations in processing conditions such as temperature and sintering pressure, (iii) chemical modifications during sintering, and (iv) fluctuations in polarization conditions and methods. In practice, a variation of 5% in the elastic properties, 10% in piezoelectric properties, and 20% in dielectric properties is considered acceptable [3]. In view of these variabilities, it becomes essential to measure the reproducibility of piezoelectric properties on a frequent basis for quality control during mass production. Typically, elaborate resonance techniques are used [3, 5]. Static and quasistatic tests can also be used; however, their precision tends to be inferior to that of the resonance techniques [3]. In some cases, such as thin films and heat-sensitive piezoelectric materials, resonance techniques can be unusable or have to be supplemented with other testing methodologies.

Instrumented indentation techniques find growing appeal for assessing the mechanical properties of small components such as thin films for which conventional testing techniques may not be applicable. The development of instrumented macro-, micro- and nanoindentors and a better understanding of contact mechanics are the two main factors responsible for this surge in interest in indentation techniques [6]. In instrumented indentation tests, the indentor load, P, is continuously recorded as a

†Present address: School of Mechanical and Production Engineering, Nanyang Technological University, Nanyang Avenue, Singapore 639798.

‡Present address: Department of Materials Science and Engineering, Carnegie–Mellon University, Pittsburgh, PA 15213, U.S.A.

§To whom all correspondence should be addressed.

function of the depth of penetration of the indentor, h, into the material. From this information, properties such as Young's modulus, yield strength, and strain hardening exponent for metallic materials, and strength and fracture toughness for brittle materials can be extracted [7].

Possible benefits of instrumented indentation for the characterization of materials include the following. (1) Probing of properties and residual stresses can be done at different size scales using commercially available nano-, micro-, and macroindentors (e.g. Refs [7–11]). (2) Pre-existing residual stresses due to processing, synthesis, surface treatments or thermal excursions can be quantified using sharp indentation [9]. (3) These procedures can be automated using computer software not only for the characterization of properties and internal stresses, but also for quality control of materials during large-volume production. These attributes of instrumented indentation also point to possibilities for developing new methods for the characterization of piezoelectric materials wherein coupled electrical–mechanical effects influence the indentation response.

Giannakopoulos and Suresh [12] have proposed a general theory for the quasistatic, normal indentation of transversely isotropic, linear piezoelectric solids. Their theoretical and finite element analysis reveal that the functional P–h relationships for this fully coupled problem have the same structure as the uncoupled mechanical problem [12]. A noteworthy observation from Ref. [12] is that the resistance of the material to penetration by the indentor depends on the electrical conductivity (i.e. on whether open-circuit or closed-circuit conditions prevail). The purpose of the present work was to investigate the use of instrumented spherical indentation of piezoelectric materials for extracting piezoelectric properties. Among the different shapes of indentors that are commonly used, spherical indentors are of particular interest because of the non-singular nature of the stress fields produced by them, which makes the analysis and testing less complex [11]. In addition, the extent of damage and plasticity is minimized by the use of spherical indentors as compared to sharp indentors.

The objective of this paper is to document the results of indentation experiments on piezoelectric materials and compare them to the predictions of the theory [12]. In particular, attention is focused on the mechanical response during indentation, i.e. P–h curves. Complimentary investigations into the electrical response during indentation of piezoelectric solid are reported elsewhere [13], where the indentation force vs the electric charge induced in the indentor were measured continuously by using a conducting steel sphere with a zero bias. These companion studies [13] in conjunction with the present work show that, by using instrumented indentation, the poling direction, the aging response, and some material properties can be determined.

This paper is organized in the following manner. Necessary theoretical background is briefly reviewed in Section 2. Selection of piezoelectric materials and experiments conducted on them are described in Section 3. Results of the experiments are presented in Section 4 and are compared with the predictions. An error analysis is presented in Section 5. A parametric analysis to identify the key parameters influencing the indentation stiffness is presented in Section 6. Implications of this work are discussed in Section 7. This paper concludes with a brief summary in Section 8.

2. THEORETICAL BACKGROUND

In this section, a brief summary of the theory of Giannakopoulos and Suresh [12] for the spherical indentation of a piezoelectric material is presented. The piezoelectric material is considered to be transversely isotropic (i.e. symmetry of ∞mm) since polycrystalline, poled piezoelectric ceramics conform to this symmetry group. The quasistatic indentation analysis deals with a frictionless interface between the spherical indentor and the flat surface of the piezoelectric substrate. For a transversely isotropic piezoelectric solid, there are five elastic (c_{ij}^E), two dielectric (ϵ_i^T) and three piezoelectric (e_{ijk}) constants [3].† Thus, there are 10 independent material constants in the problem. Key parameters which influence the indentation problem are summarized in Appendix A.

Here we consider only those results of the theory [12] which directly pertain to the force–depth (P–h) curves obtained in the experiments for different electrical boundary conditions.

2.1. Perfectly conducting indentor

If the indenting sphere, of radius R, is a perfect electrical conductor with constant electric potential $\phi = \phi_0$, the boundary conditions at the indented surface are

$$\phi(r,0) = \phi_0;\ 0 \le r \le a,\ z = 0;$$

$$D_z(r,0) = 0;\ r > a,\ z = 0. \tag{1}$$

Here r and z are the radial and normal coordinate directions schematically shown in Fig. 1. The first of these equations indicates that the potential of the sphere is also the potential of the contact area (which is a circle of radius a), whereas the second shows that the electric charge distribution, D_z, outside the contact area is zero (external charges are absorbed by the surface or by the use of electrodes). When $\phi_0 = 0$, the P–h relation is given by

†The superscripts E and T refer to properties measured with the boundary condition of constant electric flux (or closed circuit) and of constant strain (or no restraint for mechanical deformation), respectively.

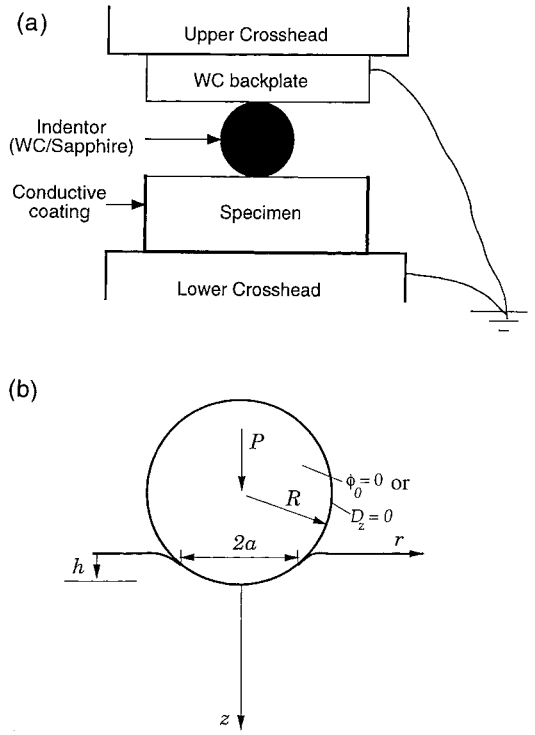

Fig. 1. Schematic representation of the experimental indentation system.

$$P = \frac{8\sqrt{R}}{3}\frac{M_4M_5 - M_3M_6}{M_1M_4 - M_2M_3}h^{3/2}. \quad (2)$$

Note that this equation provides an explicit expression for the relationship between the indentor normal force P and the depth of penetration h of the indentor into the piezoelectric material. P and h are quantities which can be directly and continuously measured during indentation. The constants M_1 through M_8 are related to the material constants and are defined in Appendix A.

2.2. Perfectly insulating indentor

For the case of the sphere being a perfect insulator with zero electric charge distribution, the boundary condition is, $D_z(r,0) = 0$; $r \geq 0$. For this case, the P–h relation is given by

$$P = \frac{8\sqrt{R}}{3}\frac{M_8M_5 - M_7M_6}{M_1M_8 - M_2M_7}h^{3/2}. \quad (3)$$

2.3. Electrically rigid specimen

If the indented material is electrically rigid, i.e. all the coupling constants are identically equal to zero, the constants M_3 and M_7 become zero and the P–h relations given by equations (2) and (3) reduce to

$$P = \frac{8\sqrt{R}}{3}\frac{M_5}{M_1}h^{3/2}. \quad (4)$$

This response is equated to the unpoled material response.

A noteworthy feature of equations (2) and (3) is that the P–h relations for conducting and insulating spherical indentors are functionally the same as that of the uncoupled mechanical case, and follow the classical Hertzian spherical indentation result for an electrically inactive ceramic, $P \sim h^{3/2}$. However, the proportionality constants are different for the unpoled, poled–conducting indentor, and poled–insulating indentor cases. This indicates that the resistance offered by the piezoelectric material to penetration by the indentor is dependent on the combination of material properties and the electrical conductivity of the indentor.

3. MATERIALS AND EXPERIMENTS

3.1. Materials

Solid solutions of a lead zirconate titanate and a barium titanate were selected for conducting the indentation experiments. The exact chemical compositions (in mol%) are $47PbTiO_3 + 47PbZrO_3 + 6SrZiO_3$ and $91.7BaTiO_3 + 8.3CaTiO_3$, respectively. The former is typically referred to as PZT-4 in the piezoelectric literature [3]. The selection of these materials was guided by the following considerations.

1. Barium titanate (BT) is a widely studied piezoelectric material and was extensively used before the advent of PZTs [3]. Currently, various solid solutions of PZTs are the materials of choice because of their high values of coupling coefficients. Among the PZTs, the use of PZT-4 is widespread. Together, PZT-4 and BT form two distinct examples; one with a high dielectric constant and the other with a low dielectric constant, thus providing two very different cases for experimental studies of indentation.
2. Because these materials are widely studied, reliable background information on all the necessary material properties, i.e. elastic, dielectric, and piezoelectric constants, are readily available. This allows for prediction of indentation stiffness without the need for invoking additional approximations.
3. Both PZT and BT can be processed with sufficient reliability to obtain reproducible microstructures and properties. Hence they are readily available from commercial sources in bulk quantities.

A material, which conforms to the specification of PZT-4, was obtained in poled and unpoled condition (commercial designation: BM400, Sensor Technology Limited, Collingwood, Ontario, Canada). Specimen dimensions were 12 mm in diameter and 3 mm in thickness. A poled BT specimen was obtained as a 100 mm diameter disk with

Table 1. Pertinent properties of the piezoelectric ceramics

Property	Lead zirconate titanate	Barium titanate
General		
Composition (in mol%)	$47PbTiO_3 + 47PbZrO_3 + 6SrZiO_3$	$91.7BaTiO_3 + 8.3CaTiO_3$
Density (10^3 kg/m^3)	7.5	5.7
Curie temperature (°C)	328	115
Elastic constants		
c_{11}^E (GPa)	139	158
c_{33}^E	115	150
c_{12}^E	77.8	69
c_{13}^E	74.3	67.5
c_{44}^E	25.6	45
c_{66}^E	30.6	45
c_{33}^D	159	177
Dielectric constants		
ϵ_{11}^T (10^{-9} F/m)	6.461	8.850
ϵ_{33}^T	5.620	8.054
Piezoelectric constants		
e_{31} (C/m^2)	−5.2	−3.1
e_{33}	15.1	13.5
e_{15}	12.7	10.9

Note: Superscripts E and D refer to elastic properties measured in short- and open-circuit conditions, respectively. Superscript T refers to dielectric constant measured with no mechanical constraint.

a thickness of 4.2 mm (commercial designation: EC55, provided by Edo ceramics, Salt Lake City, Utah, U.S.A.). Smaller specimens were cut from this slab. Unpoled BT specimens were obtained by annealing the specimen above its Curie temperature (at 150°C) in a flowing argon environment for 2 h. Relevant mechanical, dielectric, and piezoelectric properties of PZT-4 and BT were listed in Table 1. Both piezoelectric materials have an average grain size on the order of 1 μm, which is much smaller than the diameter of the imprint created by the indenter. In addition, size scales associated with the domain structures are even smaller than the indentation contact diameter.

3.2. Experiments

All the specimens were polished (on only that side on which indentation experiments were conducted) prior to testing. Note that polishing induces heavy deformation resulting in depoled surface layers. The thickness of the deformed layer is approximately equal to that of the grit of the polishing medium. This may introduce an error in the results of the indentation experiments of poled specimens. In order to minimize this error, the first polishing step involved the use of 1 μm diamond paste. The specimen was then successively polished to a finish of 0.05 μm.

In order to enforce the experimental conditions similar to the boundary conditions of zero electric potential far away from the indentor (see Section 2), the back surface (the side opposite to that being indented) and the side surfaces of the specimen were coated with gold. The lower cross-head of the mechanical test machine on which the specimen was placed and the upper cross-head (to which the indentor was attached) were both electrically grounded, thus making the potential far away from the point of contact zero. Figure 1 depicts a schematic of the indentation system illustrating these features.

Indentation experiments were conducted using an instrumented micro-indentation testing device developed in-house [7, 8]. This device allows measurements of load and the corresponding depth of penetration with a precision of 0.01 N and 0.01 μm, respectively. Details of this testing method can be found in Refs [7, 8]. Three types of indentation experiments were performed: (i) Indentation of unpoled material to capture the behavior when a coupling between electrical and mechanical response is absent (electrically rigid body). (ii) Indentation of poled material with a conducting indentor. (iii) Indentation of the poled specimen with an insulating indentor. A 10 wt% Co–WC ball indentor (Young's modulus, $E = 475$ GPa and Poisson ratio, $\nu = 0.22$) was used for the first two cases. For the insulating indentor case, a sapphire ball ($E = 378$ GPa and $\nu = 0.25$) was used. In all the cases, the radius of the indenting sphere, R, was 0.8 mm. All the tests were conducted in displacement control with a prescribed displacement rate of 2 μm/min.

3.3. Data analysis

Instantaneous load, P, and the corresponding depth of penetration of the indentor, h, were measured. In the case of purely elastic Hertzian spherical contact, the P–h relation is given by (e.g. Ref. [11])

$$P = S_1 h^{3/2},\ S_1 = \frac{4}{3}\left(\frac{1-\nu_1^2}{E_1} + \frac{1-\nu_2^2}{E_2}\right)^{-1} R^{1/2} \quad (5)$$

where E_1 and E_2 are Young's moduli, and ν_1 and ν_2

Table 2. A comparison of measured and predicted properties

Material	Condition	Indentor	Compliance, C (N/μm$^{1.5}$)	Indentation stiffness (GPa)		Relative change (%)	
				Measured	Predicted	Measured	Predicted
PZT-4	Unpoled	WC	1.67	93.5	105.1	+22.7	+21.9
	Poled	WC	1.48	76.2	86.2	0	0
	Poled	Sapphire	1.31	65.9	75.1	−13.5	−12.9
$BaTiO_3$	Unpoled	WC	2.14	150.4	150.7	−3.5	−4.2
	Poled	WC	2.18	155.8	157.3	0	0
	Poled	Sapphire	2.1	156.8	157.9	+0.6	+0.4

are Poisson's ratios of the specimen and indentor, respectively.

Because of the possibility of deformation at the back face of the indentor, however, the measured h may include the displacement due to indentation at the opposite side of the sphere. Since the applied load is the same at both contact points, the total P–h relation which accounts for this effect is given by

$$P = Sh^{3/2},\ S = \left[\left(\frac{1}{S_1}\right)^{2/3} + \left(\frac{1}{S_2}\right)^{2/3}\right]^{-3/2} \qquad (6)$$

where S_2 is the contact compliance between the back surface and the indentor and S is the total contact compliance. The value of S_2 is 9.3 and 8.4 N/μm$^{1.5}$ for the WC and sapphire ball indentors, respectively. A plot of the total compliance of the system, S, against the indentation stiffness of the specimen, $E/(1-\nu^2)$, for these two indentors is presented in Fig. 2.

The value of S is extracted from the measured P–h curves using the integration scheme proposed by Alcala *et al.* [8]. This procedure ensures precise identification of the displacement that corresponds to zero load. Note that it is essential to set the origin correctly since a relatively large displacement induces only a small increase in the load at the onset of contact. Once the value of S is extracted, the indentation stiffness of the material is obtained with the aid of Fig. 2.

Only the loading curves were used to obtain the indentation stiffness. Unloading curves were not used because both the materials exhibited some degree of hysteresis. The theoretical analysis used to interpret the results (Section 2) assumes elastic response and a linearly piezoelectric material. If this were to be true, the unloading curve should coincide with the loading curve. However, this is not the case, particularly for the PZT material. Since damage induced near the peak load just prior to unloading could not be quantitatively analyzed, only the loading curves were utilized for the analysis.

†This permanent deformation is due to the compaction and subsequent flow of the material underneath the indentor.

Each indentation experiment was repeated at least five times and only the average values are reported. For a given material–indentor system, the value of S measured is highly reproducible with variation only in the second decimal. This resulted in a standard deviation that is less than 1% of the mean value of indentation stiffness.

4. RESULTS

Experimental P–h curves obtained under unpoled, poled–insulating indentor, and poled–conducting indentor combinations for both PZT and BT are presented in Figs 3 and 4, respectively. For comparison purposes, corresponding predicted P–h curves are also plotted in Figs 3 and 4. These predictions are based on equations (2) and (3) along with an a priori knowledge of the material constants supplied by the material sources. It is seen from these figures that the trends in the P–h relations for both materials are similar to those predicted by the theory. With respect to material–indentation combination, completely opposite trends are seen in these two different materials, and these opposite trends are correctly predicted by the theory. For BT, the indentation stiffness increases (by 4.2%) when the material is poled, and within the poled cases, the stiffness is slightly higher (by 0.4%) when an insulating indentor is used.

The trends in the PZT are not only exactly opposite to the trends in the BT but the relative changes in stiffness are also more pronounced. A 22% drop in stiffness is noted when the material is poled. In between the conducting and insulating indentor cases, the stiffness is lower in the latter case by 13%. Measured and predicted values of the indentation stiffness for various material–indentor combinations are summarized in Table 2.

The PZT specimens exhibit significant inelasticity† as compared to BT which is almost elastic. Loading and unloading responses of these materials are plotted in Fig. 5 to illustrate these differences. As seen from this figure, there is a residual displacement of 0.3 μm in a poled PZT indented up to 4.8 N of load by a WC indentor. This is 13.5% of the maximum displacement (2.2 μm). The imprints of indentation could not be captured with optical

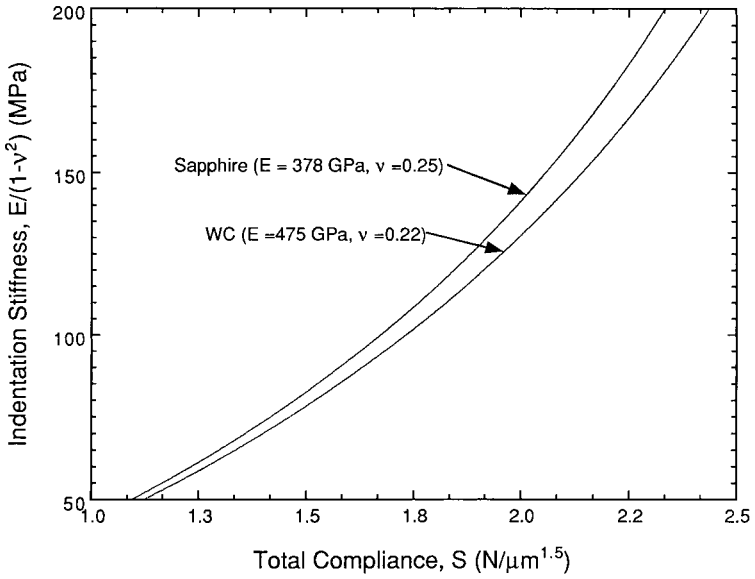

Fig. 2. Total compliance of the indentation system plotted against the indentation stiffness of the specimen for WC and sapphire indentors.

microscopy due to their very small size (calculated to be approximately equal to 42 μm).

In view of the plasticity exhibited by the PZT, only the compliance values obtained at the very beginning of the loading (P<0.5 N) were used. Even then, a 11–13% deference between predicted and measured stiffness is noted, with the measured value being consistently lower for all three indentor–material condition combinations. It is interesting to note that the difference between predicted and measured stiffnesses is approximately the same as the fraction of residual displacement in the total displacement. In the case of BT, however, neither any residual displacement (Fig. 5) nor indentation imprints were observed indicating that this material remains essentially elastic. Commensurately, the measured and experimental indentation stiffness values in BT were found to be very consistent.

From Table 2, it is seen that the relative difference predicted between poled and unpoled cases, and between the conducting and insulating indentors are in good agreement with the experimental results for both PZT and BT. Here, the value of the indentation stiffness obtained on poled material

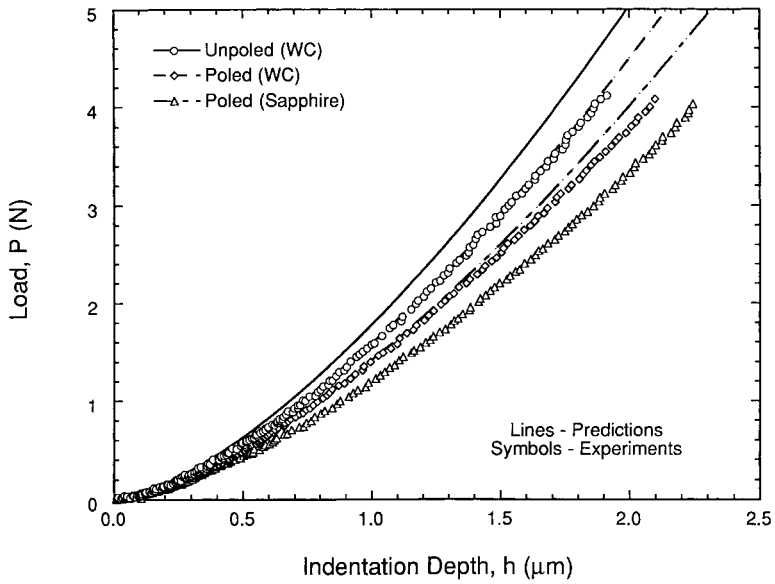

Fig. 3. Experimental and predicted P–h curves for PZT-4.

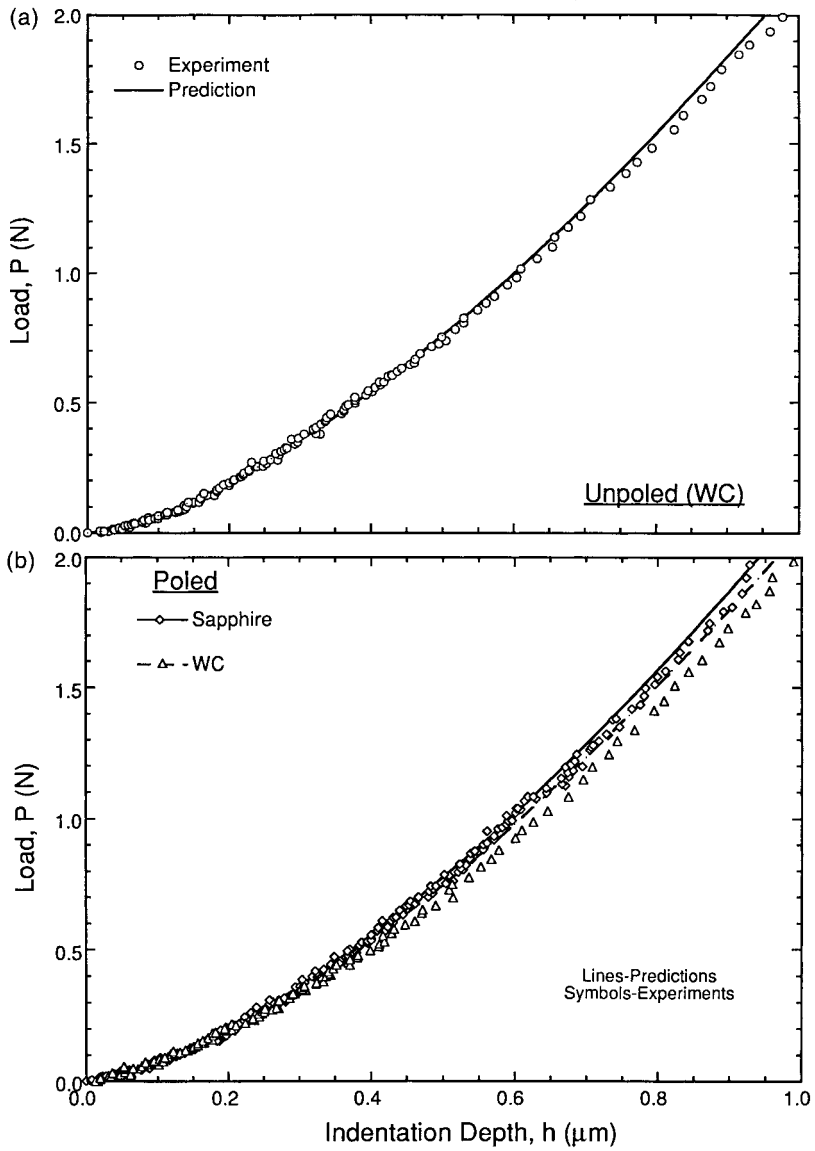

Fig. 4. Experimental and predicted P–h curves for BT in the (a) unpoled and (b) poled conditions.

with a conducting indentor has been used as the basis for calculating the relative difference. The choice is motivated by the following reason. In the theory, when the mechanical and electrical responses are uncoupled, the resulting P–h relation, equation (4), is that for the spherical indentation of a transversely isotropic solid. This is considered to be the response of the unpoled material. In reality, however, the unpoled material is isotropic. One can adopt a suitable averaging approximation to overcome this discrepancy,† a sound theoretical scheme is not available for such an approximation. On the other hand, the poled material corresponds exactly to the theoretical material; hence its response was chosen as the basis for comparison.

It is also important to note here that although the depth of penetration of the indentor into the material is small, the contact diameter spaces many dozen grains. Therefore, the indentation response reported in this paper is expected to be independent of the grain structure, pole domain dimensions and the local crystallogrphic orientations of the indented grains. On the other hand, the contact region was sufficiently far away (i.e. at least six times the contact diameter) from the edges of the indented specimen; therefore, the results reported here are not influenced by the dimensions of the specimen.

†Since the anisotropy is not very large (for example, in PZT-4 the difference between c_{33}^E and c_{11}^E is 15% whereas for BT it is only 5%), the error introduced in the indentation response of the unpoled material due to the anisotropy is insignificant. Good agreement between the predicted and experimental stiffness of the BT material validates this result.

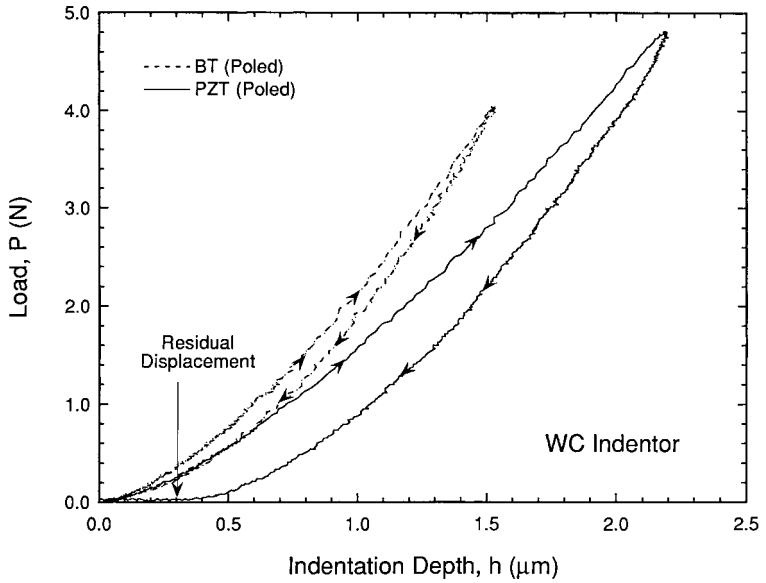

Fig. 5. A comparison of loading and unloading curves for PZT-4 and BT.

For the present experiments on polycrystalline, bulk piezoelectric ceramics, indentation by a sphere with a sufficiently large diameter is desirable since it minimizes the inelastic response of the specimen. However, for characterizing small material volumes such as piezoelectric thin films, a sharp indenter such as a cone is more suitable. Under certain geometric conditions and load levels, analysis of a cone indentation is available and has been proven valid in testing piezoelectric materials [14].

5. ERROR ANALYSIS

As noted earlier, instrumented indentation offers a potentially new tool for the characterization of electric constants. It is, therefore, of interest to quantify the sources and magnitudes of errors involved in these measurements. The theoretical analysis of the spherical indentation problem predicts the P–h relation to be of the type given by equations (2) or (3). The constant S depends on the elastic, piezoelectric and dielectric properties of the indented material. As discussed in Section 1, these properties are subject to considerable variability. Hence, it is essential to conduct an error analysis to identify key material parameters whose statistical variations directly influence the value of S and thus the *predicted* indentation stiffness value. Such variations are intrinsic to the nature of the material. On the other hand, there are errors associated with the *measured* value of S due to errors in measuring P and h. This extrinsic variability depends on the sensitivity of the measuring technique. Since, the standard deviation in S, measured using repeated experiments, is only about 1%, we assume that the error in the measured properties is negligible. To assess the error associated with the predicted value of S, an error analysis is carried out in the following using standard error propagation methods [15].

The uncertainties in the material properties were assumed to be random and uncorrelated with each other. The following is an analysis conducted on the basis of the order of magnitudes of various material constants. Note the order of magnitudes of the various material constants (expressed in the international system of units): the elastic constants are of the order of $O(10^{10})$, the piezoelectric constants are of the order of $O(1)$ and the dielectric constants are of the order of $O(10^{-9})$.

Let the standard deviation of a quantity x be denoted as σ_x^2. For the perfectly conducting indentor case, a first approximation analysis shows that

$$\sigma_S^2 \sim \frac{32}{3}\gamma_1^2\left(m_1 - \frac{m_3}{2}\right)^2 (M_4^2\sigma_{M_1}^2 + M_1^2\sigma_{M_4}^2 + M_3^2\sigma_{M_2}^2 + M_2^2\sigma_{M_3}^2) \tag{7}$$

where M_i and $\sigma_{M_i}^2$ are given in Appendix B. For the case of a perfectly insulating indentor

$$\sigma_S^2 = \frac{32}{3}((M_1M_8 - M_2M_7)^2(M_8^2\sigma_{M_1}^2 + M_1^2\sigma_{M_8}^2 + M_7^2\sigma_{M_2}^2 + M_2^2\sigma_{M_7}^2)(M_4M_5 - M_3M_6)^2 \times (M_4^2\sigma_{M_5}^2 + M_5^2\sigma_{M_4}^2 + M_3^2\sigma_{M_6}^2 + M_6^2\sigma_{M_3}^2)). \tag{8}$$

This error analysis shows that, for both the cases, the uncertainty in S is strongly influenced by the uncertainties in elastic constants, followed by the uncertainties in piezoelectric constants, whereas variations in the dielectric constants have almost no effect on S. Since the uncertainty in elastic con-

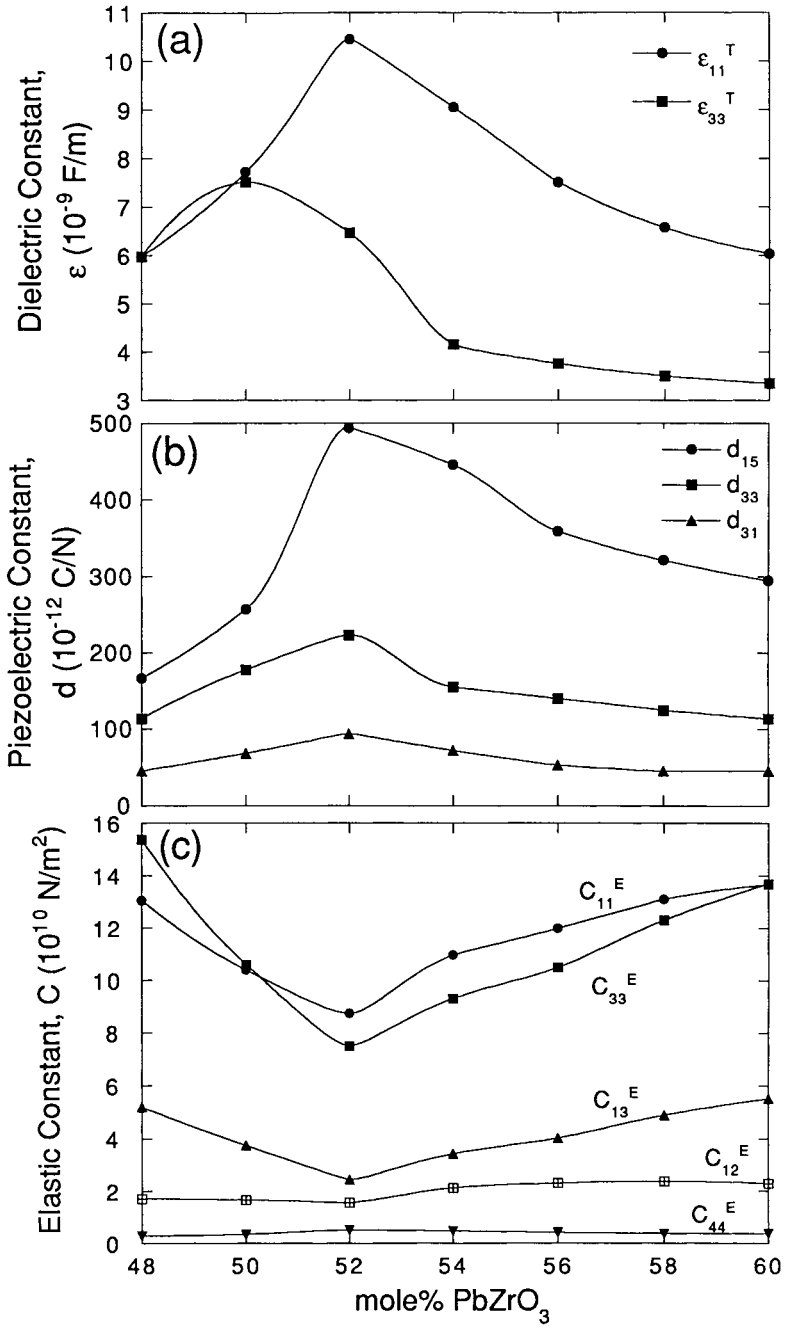

Fig. 6. The variation of dielectric, piezoelectric, and elastic constants with composition for alloys of the $Pb(Ti,Zr)O_3$ system [3].

stants is about 5% of their average values, it is expected that the uncertainty in S should be about 5% also. However, the relative differences between indentation stiffnesses of various combinations of indentor and material condition are not significantly influenced by the uncertainties in various material constants, particularly by the dielectric and piezoelectric constants. As shown in the above analysis, these properties have only secondary effects on the uncertainty in S.

While there might be a systematic difference between the absolute values of measured and predicted indentation stiffnesses (for a particular testing condition), the relative differences between indentation stiffnesses obtained with various testing combinations should not be influenced by the uncertainties in material constants. Hence, they should match well with the predicted differences. Experimental results presented in Section 4 agree well with this argument.

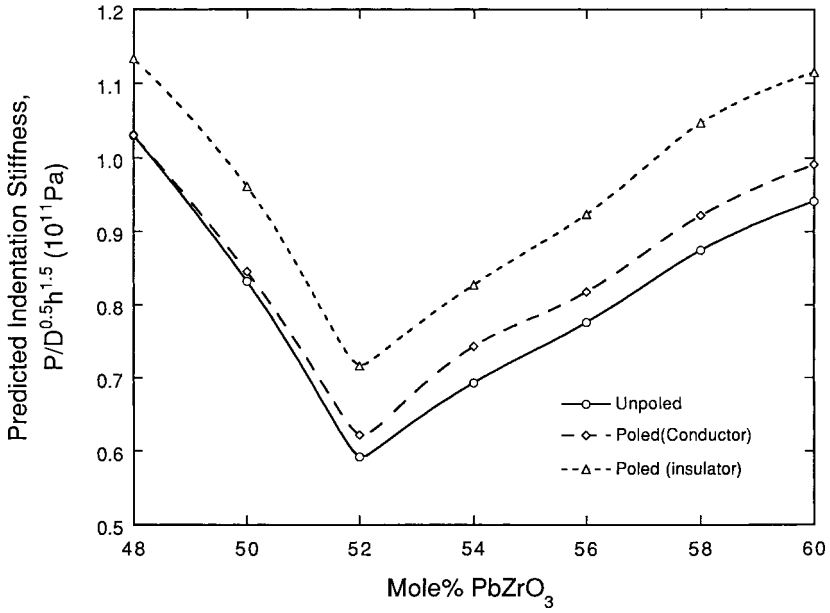

Fig. 7. Predicted variation of indentation stiffness with composition for alloys of the $Pb(Ti,Zr)O_3$ system.

6. PARAMETRIC ANALYSIS

In addition to an error analysis, a parametric analysis was also conducted in this work. The objective was to correlate the changes in the constituent material properties with variations in relative indentation response. Note that the variation in *indentation stiffness* depends on the interplay between the 10 independent material constants through the characteristic equation, equation (A1). Although a full analysis is beyond the context of this particular study, a preliminary analysis for the $PbTiO_3$–$PbZrO_3$ solid solution system was conducted in this work. This particular choice is motivated by the fact that compositional variants of this system are widely used because of their superior piezoelectric properties. In the $PbTiO_3$–$PbZrO_3$ sub-solidus phase diagram a morphotropic tetragonal–rhombohedral phase boundary exists at a composition of $46.5PbTiO_3$–$53.5PbZrO_3$ (composition in mol%) where the coupling factor and dielectric constants are the highest [3]. Variations in dielectric, piezoelectric, and elastic constants as a function of composition near this phase boundary are plotted in Fig. 6 [3].

Predicted† variations in indentation stiffness for unpoled, poled–conducting indentor, and poled–insulating indentor combinations are plotted in Fig. 7. From this figure it is seen that the predicted trends are similar to those in the elastic constants c_{11}^E, c_{33}^E, and c_{13}^E. This result is consistent with the results of error analysis presented earlier. The following additional observations are of interest.

1. The change in indentation stiffness due to polarization (defined as the difference between indentation stiffness of poled and unpoled materials with respect to the indentation stiffness of the poled material) is plotted against the elastic and dielectric anisotropies (defined as $(c_{33}^E - c_{11}^E)/c_{33}^E$ and $(\epsilon_{33}^T - \epsilon_{11}^T)/\epsilon_{33}^T$, respectively) in Figs 8(a) and (b). From these figures, it is seen that there is a nonlinear correlation between these quantities. It appears that the anisotropy in the dielectric constant also plays a role in the change of indentation stiffness when the material is poled. This is substantiated by the fact that even when the elastic anisotropy is zero, there is a significant difference between poled and unpoled indentation responses. This observation indicates that *the change in indentation stiffness when the piezoelectric ceramic is poled is not only due to the elastic anisotropy that is introduced in the material during polarization, but also due to the dielectric anisotropy*.
2. The second observation pertains to the difference in indentation stiffness between conducting and insulating indentors. One might anticipate that this difference is related to the strong piezoelectric coupling constant, d_{33}. However, within the range of parametric analysis conducted in this work, no correlation between d_{33} and the indentation stiffness is found.

In addition to the above observations, we note that the results on PZT-4 do not agree exactly with

†Note that these predictions were made using finite element analysis (FEA). The agreement between results of the FEA and the analytical model was checked for a number of cases including the two particular materials used in the experimental study. See Ref. [12] for further details.

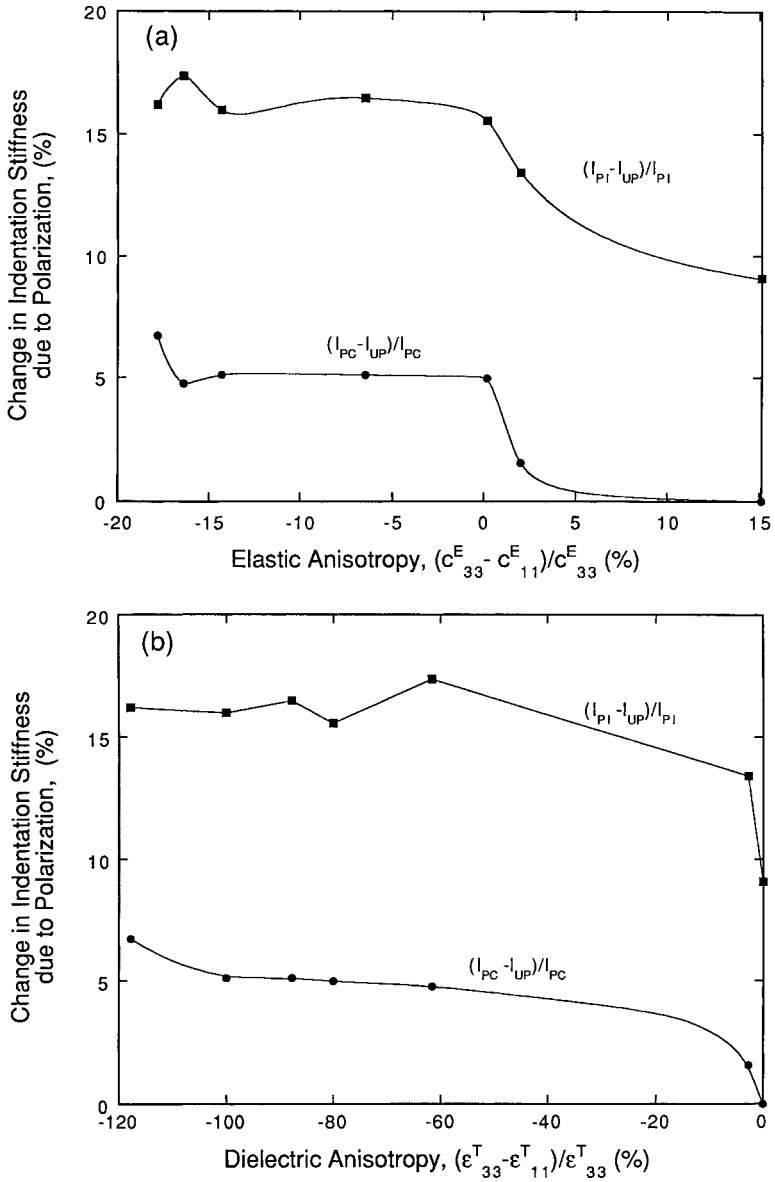

Fig. 8. Change in indentation stiffness due to polarization as a function of (a) elastic anisotropy and (b) dielectric anisotropy. I_{PI}, I_{UP} and I_{PC} refer to the indentation stiffness values for the poled substrate–insulated indentor, unpoled material, and poled substrate–conducting indentor cases, respectively.

the data from Fig. 4. This indicates that the indentation stiffness has to be evaluated on a case by case basis since it depends on all 10 material constants.

7. IMPLICATIONS

In this section, distinct features of the indentation response of piezoelectric solids are highlighted and the potential applications of the indentation technique for characterizing piezoelectric solids are discussed.

It is well known that the elastic modulus of piezoelectric materials depends on the experimental condition of electrical connectivity between the two opposite faces upon which external loading is applied [3]. The modulus measured with both the ends of the specimen that are electrically connected is generally lower than that measured with an open circuit. For example, there is a 38% difference between closed- and open-circuit elastic modulus (c^E_{33} and c^D_{33}, respectively) for the PZT-4, whereas it is 18% for the case of BT (Table 1). This increase in stiffness can be attributed to the additional mechanical resistance offered by the undissipated potential generated due to the mechanical deformation of the piezoelectric solid. In this context, it is not surprising to see a difference in indentation stiffness of the poled piezoelectric materials when the exper-

imental condition is changed from conducting to insulating indentor. However, the experimental work conducted in this study brings out some distinct features of indentation which cannot be identified through conventional testing.

1. The indentation stiffness of the poled material can be significantly different from that of the unpoled material. Note that this is not because of the change in symmetry that occurs during the poling process but it is instead related to the potential generated with deformation. If the former case were to be true, we should see a significant difference between the predicted and experimental stiffness in the unpoled case. As discussed earlier, no such difference was observed for BT (which is elastic) and PZT (the difference is accounted for by the inelasticity).
2. In the poled case, the indentation stiffness need not necessarily increase when the experimental conditions are changed from closed to open circuit, as in uniaxial testing. Depending on the material properties, a decrease in the indentation stiffness (as in the PZT) can also be observed.
3. The quantitative difference measured between open- and short-circuit cases in uniaxial testing is different to that measured in indentation.

The present work and that reported by Sridhar *et al.* [13] show that indentation can be used to estimate the piezoelectric material response both quantitatively and qualitatively. There are a number of advantages in using indentation techniques to characterize piezoelectric materials. Some of these advantages were already listed in Section 1 of this paper. Additional advantages are listed below.

1. The indentation testing technique can be used to probe newly developed materials for their properties. For example, the response of the unpoled material can be used to evaluate the elastic properties of the materials. Combinations of elastic, dielectric, and piezoelectric properties can be evaluated by conducting tests on poled material and by simply changing the type of indentor.
2. Piezoelectric materials are known to age even at room temperature. The aging response and the activation energy for depolarization of the material can be monitored readily with the indentation technique. The work of Sridhar *et al.* [13] who have investigated the depoling of BT enhanced by polarization loss due to annealing at elevated temperatures confirms this possibility. Similarly, it should be possible to monitor the quality of components that are shelved for long periods with the indentation technique to assess their usability.
3. Indentation testing is nondestructive when it is only used to obtain the P–h relations. On the other hand, indentation strength tests (i.e. the specimen is loaded until it cracks and fractures) can be used to assess fracture properties and in certain cases machinability.

8. CONCLUDING REMARKS

Spherical indentation experiments conducted on piezoelectric materials PZT-4 and BT show that the indentation stiffness depends on the material condition (poled vs unpoled) and type of indentor (conducting vs insulating) used. The experimental results are in good agreement with the theoretical predictions of Ref. [12]. A preliminary parametric analysis conducted indicates the complexity of the problem of predicting the indentation stiffness variations with a given material parameter variation. The change in indentation stiffness when the material is poled is due to the introduction of elastic and dielectric anisotropy.

This work and the parallel work of Sridhar *et al.* [13] show that instrumented indentation measurements of load, displacement, and electrical current offer a new tool for characterizing piezoelectric materials. Although the charge distribution under the indentor cannot be sustained if the contact area is fixed, the charge build-up increases during the quasistatic advance of the contact area under a steadily increasing indentation load. If the indentor is conducting and grounded, a charge builds up in the indentor opposing that developing in the specimen. This distribution of charge which changes with time manifests as a quasistatic electric current. Such a variation of current with time, along with the mechanical measurements, can be used to characterize the properties of the piezoelectric materials, monitor the aging response and shelf life, machinability, and industrial quality control during mass production.

Acknowledgements—The authors would like to acknowledge Jorge Alcala for his help with the instrumented microindentation technique, Kenji Uchino of Pennsylvania State University for many useful insights on piezoelectric materials and Don Basco of Edo ceramics for providing the BT material used in this study.

REFERENCES

1. Cady, W. G., *Piezoelectricity*. Dover, New York, 1964.
2. Uchino, K., *Piezoelectric Actuators and Ultrasonic Motors*. Kluwer, Boston, MA, 1997.
3. Jaffe, B., Cook, W. R. and Jaffe, H., *Piezoelectric Ceramics*. Academic Press, New York, 1971.
4. Newnham, R. E., Skinner, D. P. and Cross, L. E., *Mater. Res. Bull.*, 1978, **13**, 525.
5. Mason, W. P. and Jaffe, H., *Proc. Inst. Radio Engrs*, 1954, **42**, 921.
6. Nix, W. D., *Metall. Trans. A*, 1989, **20A**, 2217.
7. Suresh, S., Alcala, J. and Giannakopoulos, A. E., MIT Case No. 7280, Technology Licensing Office, Massachusetts Institute of Technology, U.S. Patent Application pending, 1996.

8. Alcala, J., Giannakopoulos, A. E. and Suresh, S., *J. Mater. Res.*, 1998, **13**, 1390.
9. Suresh, S. and Giannakopoulos, A. E., *Acta mater.*, 1998, **46**, 5755.
10. Giannakopoulos, A. E. and Suresh, S., *Scripta mater.*, in press.
11. Johnson, K. L., *Contact Mechanics*. Cambridge University Press, Cambridge, 1985.
12. Giannakopoulos, A. E. and Suresh, S., *Acta mater.*, in press.
13. Sridhar, S., Giannakopoulos, A. E., Suresh, S. and Ramamurty, U., *J. appl. Phys.*, 1999, **85**, 380.
14. Sridhar, S., Giannakopoulos, A. E. and Suresh, S., Mechanical and electrical response of piezoelectric solids due to cone indentation, submitted for publication.
15. Bevington, P. R., *Data Reduction and Error Analysis for the Physical Sciences*. McGraw-Hill, New York, 1969.

APPENDIX A

Constants used in the indentation analysis

The electromechanical coupling for the indentation of a piezoelectric solid under different electrical boundary conditions is incorportated into the theory by recourse to Hankel-type transformations [12]. The resulting formulation comprises three ordinary equations with three unknowns; a general exponential form, $\exp(-k\xi z)$, of the solution for the transformed principal variables results where ξ and z are the transformed coordinates. The parameter k must satisfy the characteristic determinant (3×3) of the system of ordinary differential equations:

$$\det[a_{ij}] = 0. \tag{A1}$$

The characteristic equation (A1) is of sixth order and has two real roots, $k = \pm k_1$ and four complex roots $k = \pm(\delta \pm \mathrm{i}\omega)$ $(i = \sqrt{(-1)})$. The coefficients of a_{ij} are given below. It is important to note that all the 10 independent constants influence the solution through the characteristic equation (1).

$$\begin{aligned} a_{11} &= c_{44}^E k^2 - c_{11}^E,\ a_{12} = -a_{21} = (c_{13}^E + c_{44}^E)k, \\ a_{22} &= c_{33}^E k^2 - c_{44}^E,\ a_{13} = a_{31} = -(e_{31} + e_{15})k_1, \\ a_{23} &= -a_{32} = -e_{33}k^2 + e_{15},\ a_{33} = \epsilon_{33}^T k_1^2 - \epsilon_{11}^T \end{aligned} \tag{A2}$$

$$\begin{aligned} \alpha_1 &= a_{12}a_{23} - a_{13}a_{22},\ \beta_1 = -a_{11}a_{23} - a_{12}a_{13}, \\ \gamma_1 &= a_{11}a_{22} + a_{12}^2 \end{aligned} \tag{A3}$$

$$\begin{aligned} \alpha_{21} + \mathrm{i}\alpha_{22} &= \alpha_1(\delta + \mathrm{i}\omega),\ \beta_{21} + \mathrm{i}\beta_{22} = \beta_1(\delta + \mathrm{i}\omega), \\ \gamma_{21} + \mathrm{i}\gamma_{22} &= \gamma_1(\delta + \mathrm{i}\omega) \end{aligned} \tag{A4}$$

$$m_1 = e_{15}\gamma_1 - c_{44}(k_1\alpha_1 + \beta_1) \tag{A5}$$

$$m_2 = e_{15}\gamma_{21} - c_{44}(\delta\alpha_{21} - \omega\alpha_{22} + \beta_{21}) \tag{A6}$$

$$m_3 = e_{15}\gamma_{22} - c_{44}(\delta\alpha_{22} + \omega\alpha_{21} + \beta_{22}) \tag{A7}$$

$$m_4 = -\epsilon_{11}\gamma_1 - e_{15}(k_1\alpha_1 + \beta_1) \tag{A8}$$

$$m_5 = -\epsilon_{11}\gamma_{21} - e_{15}(\delta\alpha_{21} - \omega\alpha_{22} + \beta_{21}) \tag{A9}$$

$$m_6 = -\epsilon_{11}\gamma_{22} - e_{15}(\delta\alpha_{22} + \omega\alpha_{21} + \beta_{22}) \tag{A10}$$

$$M_1 = \beta_1 - \beta_{22}\frac{m_1}{m_3} \tag{A11}$$

$$M_2 = \beta_{21} - \beta_{22}\frac{m_2}{m_3} \tag{A12}$$

$$M_3 = \gamma_1 - \gamma_{22}\frac{m_1}{m_3} \tag{A13}$$

$$M_4 = \gamma_{21} - \gamma_{22}\frac{m_2}{m_3} \tag{A14}$$

$$M_5 = \frac{m_1}{k_1} - \frac{m_3\delta - m_2\omega}{\delta^2 + \omega^2}\frac{m_1}{m_3} \tag{A15}$$

$$M_6 = \frac{m_2\delta + m_3\omega}{\delta^2 + \omega^2} - \frac{m_3\delta - m_2\omega}{\delta^2 + \omega^2}\frac{m_2}{m_3} \tag{A16}$$

$$M_7 = \frac{m_4}{k_1} - \frac{m_6\delta - m_5\omega}{\delta^2 + \omega^2}\frac{m_1}{m_3} \tag{A17}$$

$$M_8 = \frac{m_5\delta + m_6\omega}{\delta^2 + \omega^2} - \frac{m_6\delta - m_5\omega}{\delta^2 + \omega^2}\frac{m_2}{m_3} \tag{A18}$$

$$M_9 = \alpha_1 - \alpha_{22}\frac{m_1}{m_3} \tag{A19}$$

$$M_{10} = \alpha_{21} - \alpha_{22}\frac{m_2}{m_3}. \tag{A20}$$

APPENDIX B

Constants used in the statistical analysis

$$\begin{aligned} &a_{11} \sim c_{44}^E - c_{11}^E,\ a_{12} \sim c_{13}^E + c_{44}^E,\ a_{22} \sim c_{33}^E - c_{44}^E, \\ &a_{13} \sim -(e_{31} + e_{15}),\ a_{23} \sim -e_{33} + e_{15} \end{aligned} \tag{B1}$$

$$\begin{aligned} \alpha_1 &= a_{12}a_{23} - a_{13}a_{22},\ \beta_1 = -a_{11}a_{23} - a_{12}a_{13}, \\ \gamma_1 &= a_{11}a_{22} + a_{12}^2 \end{aligned} \tag{B2}$$

$$\begin{aligned} &m_1 \sim e_{15}\gamma_1 - c_{44}(\alpha_1 + \beta_1),\ m_2 \sim e_{15}\gamma_1 - c_{44}\beta_1, \\ &m_3 \sim e_{15}\gamma_1 - c_{44}(2\alpha_1 + \beta_1),\ m_4 \sim -e_{15}(\alpha_1 + \beta_1), \\ &m_5 \sim -e_{15}\beta_1,\ m_6 \sim -e_{15}(2\alpha_1 + \beta_1) \end{aligned} \tag{B3}$$

$$\begin{aligned} &M_1 \sim \beta_1\left(1 - \frac{m_1}{m_2}\right),\ M_2 \sim \beta_1,\ M_3 \sim \gamma_1\left(1 - \frac{m_1}{m_3}\right), \\ &M_4 \sim \gamma_1,\ M_5 \sim \frac{m_1}{2},\ M_6 \sim \frac{m_3}{2},\ M_7 \sim m_4 - \frac{m_1(m_6 - m_5)}{2m_3}, \\ &M_8 \sim \frac{m_5 + m_6}{2} \end{aligned} \tag{B4}$$

$$\begin{aligned} &\sigma_{a_{11}}^2 \sim \sigma_{c_{44}}^2 + \sigma_{c_{11}}^2,\ \sigma_{a_{12}}^2 \sim \sigma_{c_{13}}^2 + \sigma_{c_{44}}^2,\ \sigma_{a_{22}}^2 \sim \sigma_{c_{33}}^2 + \sigma_{c_{44}}^2, \\ &\sigma_{a_{13}}^2 \sim \sigma_{e_{31}}^2 + \sigma_{e_{15}}^2,\ \sigma_{a_{23}}^2 \sim \sigma_{e_{15}}^2 + \sigma_{e_{33}}^2 \end{aligned} \tag{B5}$$

$$\begin{aligned} &\sigma_{\alpha_1}^2 \sim \sigma_{a_{23}}^2 a_{12}^2 + \sigma_{a_{13}}^2 a_{22}^2,\ \sigma_{\beta_1}^2 \sim \sigma_{a_{22}}^2 a_{11}^2 + \sigma_{a_{13}}^2 a_{12}^2, \\ &\sigma_{\gamma_1}^2 \sim \sigma_{a_{11}}^2 a_{22}^2 + \sigma_{a_{22}}^2 a_{11}^2 + 2\sigma_{a_{12}}^2 a_{12}^2 \end{aligned} \tag{B6}$$

$$\sigma_{M_1}^2 \sim \beta_1^2(m_2^2\sigma_{m_1}^2 + m_1^2\sigma_{m_2}^2) + \left(1 - \frac{m_1}{m_2}\right)^2 \sigma_{\beta_1}^2,$$

$$\sigma_{M_2}^2 \sim \beta_1^2,\ \sigma_{M_3}^2 \sim \gamma_1^2(m_3^2\sigma_{m_1}^2 + m_1^2\sigma_{m_3}^2) + \left(1 - \frac{m_1}{m_3}\right)^2 \sigma_{\gamma_1}^2,$$

$$\sigma_{M_4}^2 \sim \gamma_1^2,\ \sigma_{M_5}^2 \sim \sigma_{m_1}^2,\ \sigma_{M_6}^2 \sim \sigma_{m_3}^2,$$

$$\sigma_{M_7}^2 \sim \sigma_{m_4}^2 - (m_6 - m_5)^2(m_1^2\sigma_{m_3}^2 + m_3^2\sigma_{m_1}^2) + \left(\frac{m_1}{m_3}\right)^2 (\sigma_{m_6}^2 + \sigma_{m_5}^2),\ \sigma_{M_8}^2 \sim \sigma_{m_5}^2 + \sigma_{m_6}^2. \quad \text{(B7)}$$